DØnote 5489-CONF

Search for the Higgs boson in $H \to WW^* \to e\mu$ decays at DØ in Run IIb

The DØ Collaboration
URL http://www-d0.fnal.gov
(Dated: September 6, 2007)

A search for the Higgs boson is presented in $H \to WW^* \to e^{\pm}\mu^{\mp}$ decays in $p\overline{p}$ collisions at a center-of-mass energy of $\sqrt{s} = 1.96$ TeV. The data, corresponding to an integrated luminosity of ~ 0.64 fb^{-1}analyzed here, have been collected from June 2006 to April 2007 with the Run IIb DØ detector. The data is combined with a previous result from a non overlapping data set. No excess above the standard model background has been observed and limits on the production cross section times branching ratio $\sigma \times BR(H \to WW^*)$ are presented. The combined result uses a total lumionsity of 1.7 fb^{-1}with correspondingly better sensitivity than either analysis alone.

Preliminary Results for Summer 2007 Conferences

I. INTRODUCTION

In the standard model (SM) the Higgs boson is crucial to the understanding of electroweak symmetry breaking and the mass generation of electroweak gauge bosons and fermions. Direct searches at the CERN e^+e^- collider (LEP) yield a lower limit for the Higgs boson mass of $m_H > 114.4\,\text{GeV}$ [1] at 95% CL. Indirect measurements via fits to the electroweak precision data give an upper bound of $m_H < 144\,\text{GeV}$ [2] at 95% confidence limit.

In this note a search for Higgs bosons decaying to the WW^* final state in the DØ experiment at the Tevatron is presented. To achieve a good signal-to-background ratio, the leptonic decay mode $H \to WW^* \to e^\pm\mu^\mp$ is considered, leading to final states with one electron, one muon and missing transverse momentum. This decay mode provides the largest sensitivity for the standard model Higgs boson search at the Tevatron at a mass of $M_H \sim 160$ GeV [3–5]. If combined with searches exploiting the WH and ZH associated production, this decay mode increases the sensitivity for the Higgs boson searches in the low mass region $M_H \sim 120$ GeV.

Upper limits on the $H \to WW^* \to e^\pm\mu^\mp$ cross section have already been presented in Ref. [6, 7]. In the present analysis data from Run IIb is used; however, so far only the $e^\pm\mu^\mp$ final state has been considered. Upper limits on the production cross section times branching ratio $\sigma \times BR(H \to WW^*)$ are presented. The data sample used in this analysis has been collected between June 2006 and April 2007 by the Run IIb DØ detector at the Fermilab Tevatron collider at $\sqrt{s} = 1.96$ TeV, corresponding to an integrated luminosity of ~ 0.64 fb^{-1}. This result using Run IIb data is combined with existing results using Run IIa data for the final result quoted here, giving a total data sample of 1.7 fb^{-1}.

II. THE DØ DETECTOR

We briefly describe the main components of the DØ Run IIb detector [8] important to this analysis. The central tracking system consists of a silicon microstrip tracker (SMT) and a central fiber tracker (CFT), both located within a 2.0 T axial magnetic field. The SMT strips have a typical pitch of 50–80 μm, and the design is optimized for tracking and vertexing over the pseudorapidity range $|\eta| < 3$, where $\eta = -\ln(\tan\frac{\theta}{2})$ with polar angle θ. The system has a six-barrel longitudinal structure, with each barrel a set of four silicon layers arranged axially around the beam pipe, interspersed with sixteen radial disks. The CFT has eight thin coaxial barrels, each supporting two doublets of overlapping scintillating fibers of 0.835 mm diameter, one doublet parallel to the beam axis, the other alternating by $\pm 3^\circ$ relative to the beam axis.

A liquid-argon/uranium calorimeter surrounds the central tracking system and consists of a central calorimeter (CC) covering to $|\eta| \approx 1.1$, and two end calorimeters (EC) extending coverage for $|\eta| < 4.2$, each housed in separate cryostats [9]. Scintillators between the CC and EC cryostats provide sampling of showers for $1.1 < |\eta| < 1.4$.

The muon system is located outside the calorimeters and consists of a layer of tracking detectors and scintillation trigger counters inside toroid magnets which provide a 1.8 T magnetic field, followed by two similar layers behind each toroid. Tracking in the muon system for $|\eta| < 1$ relies on 10 cm wide drift tubes [9], while 1 cm mini-drift tubes are used for $1 < |\eta| < 2$ [10].

The $H \to WW^* \to e^\pm, \mu^\mp$ candidates are selected by triggering on single or di-lepton events using a three level trigger system. The first trigger level uses hardware to select electron candidates based on energy deposition in the electromagnetic part of the calorimeter and selects muon candidates formed by hits in two layers of the muon scintillator system. Digital signal processors in the second trigger level form muon track candidate segments defined by hits in the muon drift chambers and scintillators. At the third level, software algorithms running on a computing farm and exploiting the full event information are used to make the final selection of events which are recorded for offline analysis.

III. EVENT SELECTION

In the further offline analysis electrons are identified by electromagnetic showers in the calorimeter. These showers are chosen by comparing the longitudinal and transverse shower profiles to those of simulated electrons. The showers must be isolated, deposit most of their energy in the electromagnetic part of the calorimeter, and pass a likelihood criterion that includes a spatial track match and, in the CC region, an E/p requirement, where E is the energy of the calorimeter cluster and p is the momentum of the track. All electrons are required to be in the pseudorapidity range $|\eta| < 3.0$. The transverse momentum measurement of the electrons is based on calorimeter cell energy information.

Muon tracks are reconstructed from hits in the wire chambers and scintillators in the muon system and must match a track in the central tracker. To select isolated muons, the scalar sum of the transverse momentum of all tracks other than that of the muon in a cone of $\mathcal{R} = 0.5$ around the muon track must be less than 4 GeV, where

$\mathcal{R} = \sqrt{(\Delta\phi)^2 + (\Delta\eta)^2}$ and ϕ is the azimuthal angle. Muon detection is restricted to the coverage of the muon system $|\eta| < 2.0$. Muons from cosmic rays are rejected by requiring a timing criterion on the hits in the scintillator layers as well as applying restrictions on the position of the muon track with respect to the primary vertex.

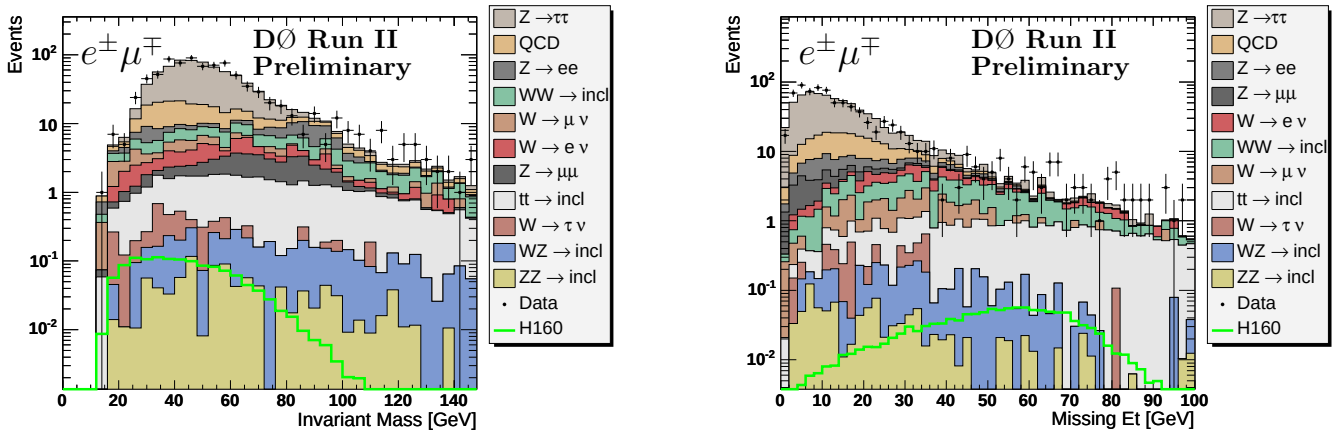

FIG. 1: Distribution of the invariant mass $M_{e^{\pm}\mu^{\mp}}$ (left) and the distribution of the missing transverse energy $\not\!\!E_{\rm T}$ after the initial transverse momentum and di-lepton invariant mass cuts (Cut 1, preselection).

Selection criterion	Value
Cut 1 Preselection	ID, leptons with opposite charge and $p_T^e > 15$ GeV and $p_T^\mu > 10$ GeV, $m_{e\mu} > 15$ GeV (remove events with 2e or 2μ if 75 GeV $< M_{e\mu} <$ 105 GeV)
Cut 2 Missing transverse energy $\not\!\!E_{\rm T}$	$\not\!\!E_{\rm T} > 20$ GeV
Cut 3 $\not\!\!E_T^{\rm Scaled}$	$\not\!\!E_T^{\rm Scaled} > 7$ (for $N_{Jet} > 0$)
Cut 4 $M_{min}^T\ (l, \not\!\!E_{\rm T})$	$M_{min}^T\ (l, \not\!\!E_{\rm T}) > 45\ GeV (M_H = 120\ GeV)$ $M_{min}^T\ (l, \not\!\!E_{\rm T}) > 50\ GeV (M_H = 140\ GeV)$ $M_{min}^T\ (l, \not\!\!E_{\rm T}) > 55\ GeV (M_H = 160\ GeV)$ $M_{min}^T\ (l, \not\!\!E_{\rm T}) > 60\ GeV (M_H = 180\ GeV)$ $M_{min}^T\ (l, \not\!\!E_{\rm T}) > 65\ GeV (M_H = 200\ GeV)$
Cut 5 Invariant mass $M_{e\mu}$	$M_{e\mu} < M_H/2$ GeV
Cut 6 Sum of $p_T^l + p_T^{l'} + \not\!\!E_{\rm T}$	$M_H/2 + 20$ GeV $< p_T^l + p_T^{l'} + \not\!\!E_{\rm T} < M_H$
Cut 7 H_T (scalar sum of p_T^{Jet})	$H_T < 100$ GeV

TABLE I: Summary of the selection criteria for a the different Higgs masses.

The decay of two W bosons into electrons or muons results in three different final states $e^+e^- + X$ (ee channel), $e^{\pm}\mu^{\mp} + X$ ($e\mu$ channel), and $\mu^+\mu^- + X$ ($\mu\mu$ channel), each of which consists of two oppositely charged isolated high transverse momentum, p_T, leptons and large missing transverse energy, $\not\!\!E_{\rm T}$, due to the escaping neutrinos. The event kinematics change significantly as a function of Higgs mass. The analysis sensitivity is improved by using selection requirements which depend on the Higgs mass, thereby reflecting the changing kinematics [3].

In the considerd $e^{\pm}\mu^{\mp}$final state, the two leptons originating from the same vertex are required to be of opposite charge, and must have $p_T^e > 15$ GeV for the electron and $p_T^\mu > 10$ GeV for muon. In addition, the di-lepton invariant mass is required to exceed 15 GeV (Cut 1, preselection). In Fig. 1 the comparison between data and Monte Carlo (MC) is shown for the invariant mass of the dilepton system and the missing transverse energy at the preselection level. Figure 2 shows the good agreement between data and MC in $\Delta\phi_{e^{\pm}\mu^{\mp}}$ distribution after applying the lepton transverse momentum and di-lepton invariant mass cuts. The background is largely dominated by Z/γ^* production which is suppressed by requiring the missing transverse energy $\not\!\!E_{\rm T}$ to be greater than 20 GeV (Cut 2). Events

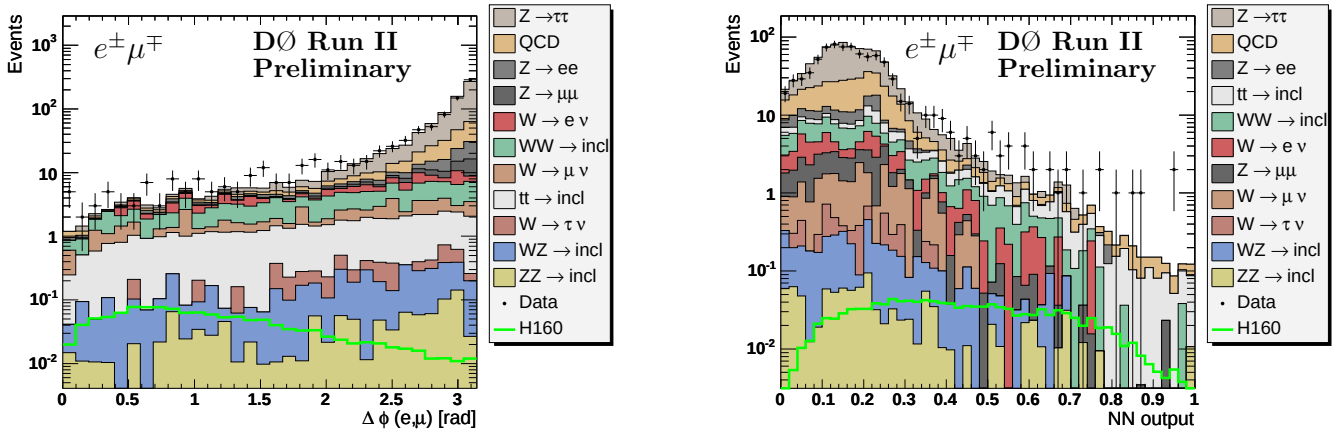

FIG. 2: Distribution of the opening angle $\Delta\phi_{e^{\pm}\mu^{\mp}}$ (left) and the output of the neural network after applying the initial transverse momentum and di-lepton invariant mass cuts (Cut 1). The expected signal for the standard model Higgs of mass 160 GeV is also shown.

are further removed if the $\not\!\!E_{\rm T}$ could have been produced by a mis-measurement of jet energies. The fluctuation in the measurement of jet energy in the transverse plane can be approximated by $\Delta E^{\rm jet} \cdot \sin\theta^{\rm jet}$ where $\Delta E^{\rm jet}$ is proportional to $\sqrt{E^{\rm jet}}$. The opening angle $\Delta\phi\,({\rm jet}, \not\!\!E_{\rm T})$ between this projected energy fluctuation and the missing transverse energy provides a measure of the contribution of the jet to the missing transverse energy. The scaled missing transverse energy defined as:

$$\not\!\!E_T^{\rm Scaled} = \frac{\not\!\!E_{\rm T}}{\sqrt{\sum_{i=jets} \left(\Delta E^{\rm i} \cdot \sin\theta^{\rm i} \cdot \cos\Delta\phi\,({\rm i}, \not\!\!E_{\rm T})\right)^2}} \tag{1}$$

is required to be greater than 7 (Cut 3).

The cuts on the minimal transverse mass $M^T_{min}(l, \not\!\!E_{\rm T})$ between the lepton and the missing transverse energy (Cut 4), the invariant mass of the dilepton system (Cut 5) and the sum of the lepton transverse momenta plus the missing transverse energy (Cut 6) are Higgs mass dependent and optimized to further suppress contributions from Z/γ^*, WW, WZ, ZZ, $W \to l\nu$ backgrounds. The minimal transverse mass $M^T_{min}(l, \not\!\!E_{\rm T})$ of either lepton and $\not\!\!E_{\rm T}$ (Cut 4) in the event $M^T_{min}(l, \not\!\!E_{\rm T}) = \sqrt{2p_T^l \not\!\!E_{\rm T}\,(1 - \cos\Delta\phi(l, \not\!\!E_{\rm T}))}$ is required to be more than 45, 50, 55, 60, 65 GeV for the Higgs masses 120, 140, 160, 180 and 200 GeV, respectively. Since the charged lepton system and the two neutrinos are emitted back–to–back, the invariant mass for the Higgs decays is restricted to $M_H/2$. Thus, depending on the Higgs mass M_H the invariant mass $M_{e^{\pm}\mu^{\mp}}$ is required to be $M_{e^{\pm}\mu^{\mp}} < M_H/2$ (Cut 5). The sum of the lepton transverse momentum p_T and the missing transverse momentum $\not\!\!E_{\rm T}$ is required to be in the range $M_H/2 + 20\,{\rm GeV} < p_T^l + p_T^{l'} + \not\!\!E_{\rm T} < M_H$ (Cut 6). $t\bar{t}$ events are further rejected by a cut on $H_T < 100$ GeV, in which H_T is the scalar sum of the p_T of good jets in the event (Cut 7).

Finally, the spin correlations in the decay of the Higgs boson are used. The leptons of the Higgs decay tend to have a small opening angle, whereas leptons from most of the backgrounds are expected to be back-to-back. In Fig. 2 on the left side the distribution of the lepton opening angle in the transverse plane $\Delta\phi_{e^{\pm}\mu^{\mp}}$ is shown after the pre-selection (Cut 1). This variable together with transverse momenta of the leptons, the invariant mass, the missing transverse energy $\not\!\!E_{\rm T}$, the angles between the leptons and the $\not\!\!E_{\rm T}$ and the minimum of both transverse mass of the leptons and $\not\!\!E_{\rm T}$ are used to build a neural net to discriminate signal versus background. The most important background is WW, as can be seen in Fig. 3 on the left side. Therefore the neural net is trained considering only this as background. The output variable of the NN is shown after Cut 1 on the right side in Fig. 2.

IV. BACKGROUNDS

The signal and standard model background processes have been generated with PYTHIA 6.319 [11] using the CTEQ6.1M parton distribution functions, followed by a detailed GEANT-based [12] simulation of the DØ detector. Using the NLO cross sections calculated with HDECAY [13] and HIGLU [14] and branching fractions BR of 0.1072 ± 0.0016 for $W \to e\nu$ and 0.1057 ± 0.0022 for $W \to \mu\nu$ [15], the expected number of events for $H \to WW^* \to e^{\pm}\mu^{\mp}$ is

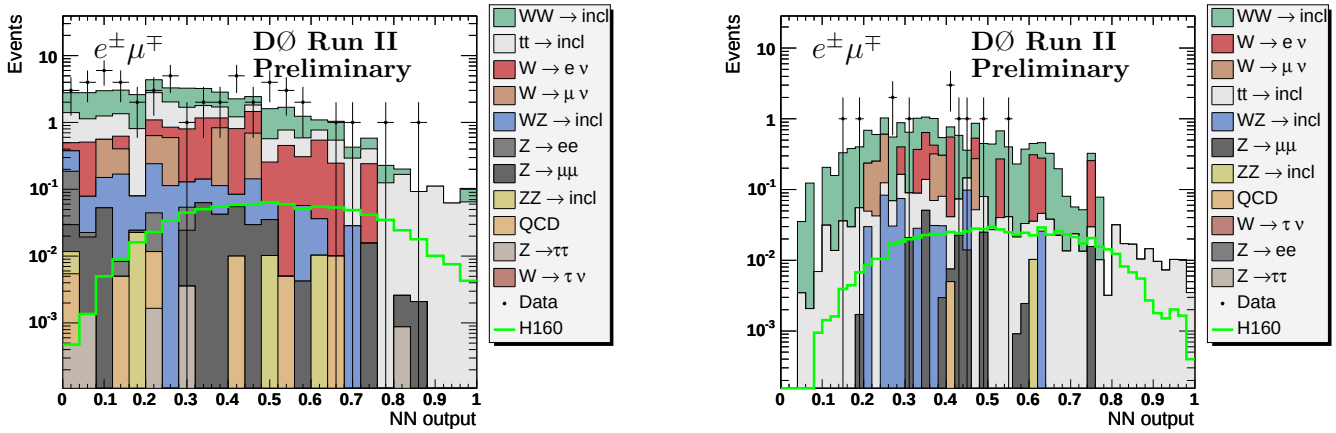

FIG. 3: Distribution of the neural network output after Cut 4 (left) and after the final selection (Cuts 1-7). The expected signal for the standard model Higgs of mass 160 GeV is also shown.

TABLE II: Number of signal and background events expected and number of events observed after the H_T selection cut is applied. Only statistical uncertainties are given.

M_H (GeV)	120	140	160	180	200
$H->WW^*$	0.117 ± 0.00002	0.444 ± 0.0001	0.69 ± 0.0001	0.543±0.0001	0.237 ± 0.00003
$Z/\gamma \to ll$	0.73 ± 0.11	0.48 ± 0.10	0.15 ± 0.01	0.06 ± 0.01	0.06 ± 0.01
Diboson (ZZ, WZ, WW)	7.2 ± 0.011	9.83 ± 0.14	10.47 ± 0.15	9.76 ± 0.14	7.89 ± 0.13
$t\bar{t}$	0.28 ± 0.01	0.73 ± 0.01	1.4 ± 0.01	1.9 ± 0.01	2.2 ± 0.01
W+jet/γ	5.62 ± 1.00	4.7 ± 0.7	4.3 ± 0.7	3.7 ± 0.7	3.7 ± 0.7
Multijet	0.04 ± 0.001	0.01 ± 0.0001	0.005 ± 0.0004	0	0
Background sum	13.9 ± 0.7	15.9 ± 0.656	16.5 ± 0.632	15.4 ± 0.588	13.9 ± 0.582
Data	12	15	13	13	9

0.38 ± 0.01(stat) events for a Higgs boson mass $M_H = 160$ GeV. The expected signal for all considered Higgs masses is given by the first line of Table II.

The $Z/\gamma \to ll$ cross section is calculated with CTEQ6.1M PDFs as $\sigma(Z/\gamma \to ll) = \sigma_{LO} \times K_{QCD}(Q^2)$ (with Q^2. the momentum transfer), with the LO cross section calculated by Pythia LO PDF and the K_{QCD} at NNLO with NLO PDF, calculated according to [16, 17]. The cross section times branching ratio of $Z/\gamma \to ll$ production in the invariant mass region 60 GeV $< M_{e^{\pm}\mu^{\mp}} <$ 130 GeV is $\sigma \times BR = 241.6$ pb. The $W \to e\nu$ background level is calculated with NNLO corrections and CTEQ6.1M as listed in [17]. For inclusive W boson production with decays into a single lepton flavor state this value is $\sigma \times BR = 2583$ pb. The calculations of Ref. [18] are used for $t\bar{t}$ production with $\sigma \times BR = 0.076$ pb with single flavor lepton decays of both W bosons. The NLO WW, WZ and ZZ production cross section values are taken from Ref. [19] with $\sigma \times BR = 0.15$ pb for WW, $\sigma \times BR = 0.014$ pb for WZ and $\sigma \times BR = 0.002$ pb for ZZ production with decay into a single lepton flavor state. The background due to multijet production, when a jet is misidentified as an electron, is determined from the data using a sample of like-sign di-lepton events with inverted lepton quality cuts (called QCD fakes in Figs. 2).

The data sample size is determined by normalizing the electron-muon invariant mass distribution (see Fig. 1) to the NNLO $Z/\gamma^* \to \tau\tau \to e^{\pm}\mu^{\mp}$ cross section. The estimated data sample size was found to be of the order of ~ 0.64 fb^{-1}. Data/MC electron and muon correction factors have been applied to MC before normalization to $Z/\gamma^* \to \tau\tau \to e^{\pm}\mu^{\mp}$. By using this method to estimate data sample size, the limit on the $H \to WW^* \to e^{\pm}\mu^{\mp}$ cross section is calculated relative to the NNLO $Z/\gamma^* \to ll$ cross section. Systematic errors, coming from the luminosity determination, on data/MC correction factors are canceled by using such a normalization procedure.

A summary of the background contributions together with signal expectations and events observed in the data after the final selection is shown in Table II. Since after all selection cuts the remaining candidate events are consistent with the background expectation, limits on the production cross section times branching ratio $\sigma \times BR(H \to WW^*)$ are derived using a method described in Ref. [20]. This method calculates the cross section limits at 95% C.L. with the integrated luminosity, number of background events, signal acceptance and number of events in data with corresponding errors as inputs. The uncertainty on the background was determined from the statistical and systematic

TABLE III: Combined observed and expected upper limits at 95% C.L. cross section ratio for $\sigma \times BR(H \to WW^*)$ and $e^{\pm}\mu^{\mp}$ final states for different Higgs boson masses M_H.

M_H (GeV)	120	140	160	180	200
Observed upper Limit ratio	38.2	11.8	3.5	5.1	10.4
Expected upper Limit ratio	37.3	11.2	5.5	8.4	18.2

uncertainty.

V. LIMIT SETTING

Various sources of systematic uncertainties affect the background estimation and the signal efficiency of H $\to WW^*$ production in $e^{\pm}\mu^{\mp}$ final states: theoretical uncertainty of WW, $t\overline{t}$ and Z/γ^* production cross sections, Jet Energy Scale (JES), electron and muon reconstruction efficiencies and resolutions. In the low mass region, the uncertainty is dominated by the jet energy scale and variations in the $W + jet/\gamma$ contribution. With increasing Higgs mass, this uncertainty is decreasing because of the decreasing contribution of $W + jet/\gamma$ events. Since the WW production is the dominant background for Higgs bosons above $M_H = 160$ GeV, the systematic uncertainty is dominated by the error on the WW production cross section. Until the systematic errors are completely studied, systematic errors of 10 % and 15 % for the signal and background respectively, based on the previous results [6], are used. The systematic uncertainty on the luminosity normalization factor is taken to be 5 %. It results from the NNLO $Z/\gamma^* \to ll$ cross section uncertainty (3.6 %) and statistical error on data/MC normalization factor of ~ 3 %.

Table III presents the expected and observed upper limits at 95% C.L on the cross section times branching ratio for different Higgs boson masses M_H. The limit is obtained by using the NN output show in Fig. 3 (for 160 GeV Higgs mass) combined with the 1 fb^{-1}limit obtained in [7]. For setting and combining the limit the procedure described in [21] has been followed. The limits are combined using the CL_s method with a log-likelihood ratio. Systematics are treated as uncertainties on the expected number of signal an background events, not on the outcome of the limit calculations. The CL_s approach here utilizes binned final-variable distributions (in our case it is the output of the neural net) rather than a single bin (fully integrated) value.

Figure 4 shows the calculated expected and observed cross section limit ratios for $\sigma \times BR(H \to WW^*)$ for the different Higgs boson masses. In Fig. 5 the absolute combined expected and observed limits are shown for the different Higgs boson masses.

VI. SUMMARY

A search for the Higgs boson is presented in $H \to WW^* \to e^{\pm}\mu^{\mp}$ decays in $p\overline{p}$ collisions at a center-of-mass energy of $\sqrt{s} = 1.96$ TeV. The data, collected from June 2006 to April 2007 with the Run IIb DØ detector, correspond to an integrated luminosity of the order of ~ 0.64 fb^{-1}. The number of events observed is consistent with expectations from standard model backgrounds. The data analysed here is combined with a previous result from a non overlapping data set. The combined result uses a total lumionsity of 1.7 fb^{-1}for the $H \to WW^* \to e^{\pm}\mu^{\mp}$ channel on the production cross section times branching ratio $\sigma \times BR(H \to WW^*)$.

Acknowledgements

We thank the staffs at Fermilab and collaborating institutions, and acknowledge support from the DOE and NSF (USA); CEA and CNRS/IN2P3 (France); FASI, Rosatom and RFBR (Russia); CAPES, CNPq, FAPERJ, FAPESP and FUNDUNESP (Brazil); DAE and DST (India); Colciencias (Colombia); CONACyT (Mexico); KRF and KOSEF (Korea); CONICET and UBACyT (Argentina); FOM (The Netherlands); Science and Technology Facilities Council (United Kingdom); MSMT and GACR (Czech Republic); CRC Program, CFI, NSERC and WestGrid Project (Canada); BMBF and DFG (Germany); SFI (Ireland); The Swedish Research Council (Sweden); CAS and CNSF

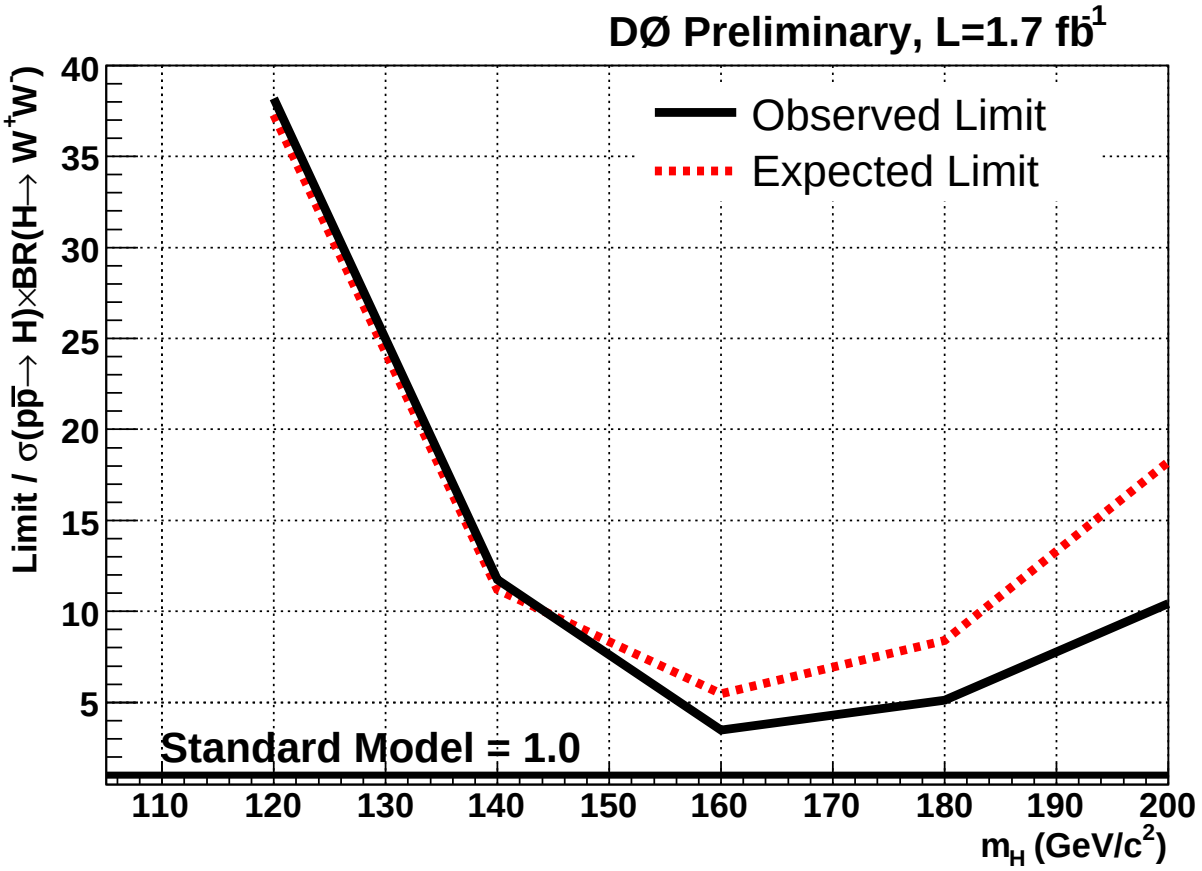

FIG. 4: Expected and observed 95% CL cross section ratio of the combined Run IIa and Run IIb analyses for $H \to WW^*$.

(China); Alexander von Humboldt Foundation; and the Marie Curie Program.

[1] R. Barate *et al.*, Phys. Lett. B **565** (2003) 61.
[2] The LEP Collaborations, the LEP Electroweak Group, the SLD Electroweak and Heavy Flavours Group, [March 2007 update].
[3] T. Han, A. Turcot, R-J. Zhang, Phys. Rev. D. 59, 093001 (1999).
[4] M. Carena *et al.* [Higgs Working Group Collaboration], "Report of the Tevatron Higgs working group", hep-ph/0010338.
[5] K. Jakobs, W. Walkowiak, ATLAS Physics Note, ATL-PHYS-2000-019.
[6] DØ Collaboration, V. Abazov *et al.*, Phys. Rev. Lett. 96, 011801 (2006)
[7] DØ Collaboration, Conference Note 5063.
[8] DØ Collaboration, V. Abazov *et al.*, to be published in Nucl. Instrum. Methods A; arXiv:physics/0507191.
[9] DØ Collaboration, S. Abachi *et al.*, Nucl. Instrum. Methods Phys. Res. A **338**, 185 (1994).
[10] V. Abramov *et al.*, Nucl. Instrum. Meth. A **419**, 660 (DØ Collaboration,1998).
[11] T. Sjöstrand *et al.*, Comp. Phys. Comm. **135**, 238 (2001).
[12] R. Brun and F. Carminati, CERN Program Library Long Writeup W5013, 1993 (unpublished).
[13] A. Djouadi et al., Comput. Phys. Commun. **108**, 56 (1998).
[14] M. Spira, Report DESY T-95-05 (October 1995), arXiv:hep-ph/9510347.
[15] Particle Data Group, S. Eidelman *et al.*, Phys. Lett. B **592**, 1 (2004).
[16] R. Hamberg, W.L. van Neerven, and T. Matsuura, Nucl. Phys. **B359**, 343 (1991) [Erratum-ibid. **B644**, 403 (2002)].
[17] T. Nunnemann, DØ Note 4476.
[18] N. Kidonakis and R. Vogt, Phys. Rev. D **68**, 114014 (2003).
[19] J. M. Campbell and R. K. Ellis, Phys. Rev. D **60**, 113006 (1999).
[20] T. Junk, Nucl. Instr. and Meth., A434(1999) 435.
[21] DØ Collaboration, Fermilab-TM-2386-E.

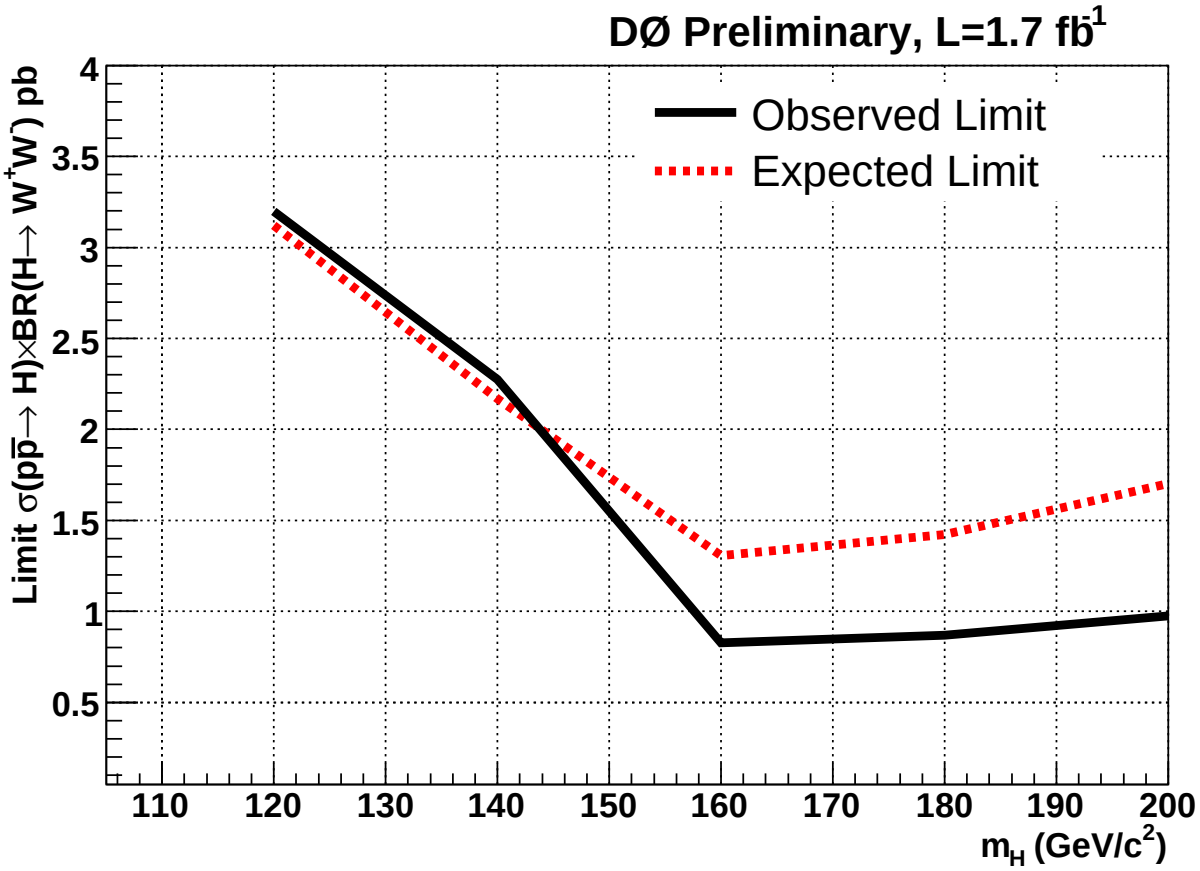

FIG. 5: Expected and observed 95% CL limit of the combined Run IIa and Run IIb analyses for $H \to WW^* -> e^{\pm}\mu^{\mp}$.